Study of Enzymatic Digestion of Cellulose by Small Angle Neutron Scattering

Article *in* Biomacromolecules · February 2010

DOI: 10.1021/bm9008952 · Source: PubMed

Study of Enzymatic Digestion of Cellulose by Small Angle Neutron Scattering

M. S. Kent,*[,†,‡] G. Cheng,[‡,§] J. K. Murton,[†,‡] E. L. Carles,[†,‡] D. C. Dibble,[‡,§] F. Zendejas,[§] M. A. Rodriquez,[†] H. Tran,[‡,§] B. Holmes,[‡,§] and B. A. Simmons[‡,§]

Sandia National Laboratories, P.O. Box 5800, Albuquerque, New Mexico 87123, Sandia National Laboratories, P.O. Box 969, Livermore, California 94551, and Joint BioEnergy Institute, 5885 Hollis Street, Emeryville, California 94608

B. Knierim[‡,||] and M. Auer[‡,||]

Lawrence Berkeley National Laboratory, 1 Cyclotron Road, Berkeley, California 94720

J. L. Banuelos[⊥] and J. Urquidi[⊥]

New Mexico State University, Box 30001 MSC 3A, Las Cruces, New Mexico, 88003

R. P. Hjelm[#]

Los Alamos National Laboratories, P.O. Box 1663, Los Alamos, New Mexico 87545

Received August 6, 2009; Revised Manuscript Received November 6, 2009

Small angle neutron scattering (SANS) was used to study the structure of Avicel (FD100) microcrystalline cellulose during enzymatic digestion. Digestions were performed in either of two modes: a static, quiescent mode or a dynamic mode using a stirred suspension recycled through a flow cell. The scattering pattern for as-received Avicel in D_2O buffer is comprised of a low Q power law region resulting from the surface fractal character of the microcrystalline fibers and a high Q roll-off due to scattering from water-filled nanopores with radii ~20 Å. For digestions in the dynamic mode the high Q roll-off decreased in magnitude within ~1 h after addition of enzymes, whereas in the static digestions no change was observed in the high Q roll-off, even after 60 h. These results indicate that only with significant agitation does enzyme digestion affect the structure of the nanopores.

Introduction

The breakdown of cellulose into fermentable sugars is a critical step in the production of renewable transportation biofuels derived from the biological conversion of biomass.[1–3] The most common route is through enzymatic digestion. Improving the efficiency of enzymatic hydrolysis of cellulose is one of the key technological hurdles in reducing the cost of producing ethanol from cellulosic feedstocks.[4] While the presence of lignin is an important factor limiting the yields of fermentable sugars from biomass,[5] the present study focused on purified natural cellulose in the absence of lignin in order to develop a fundamental understanding of the mechanisms of cellulose hydrolysis.

The rate of enzymatic hydrolysis of purified natural cellulose decreases with time, and, depending upon conditions, yields of fermentable sugars can be far less than 100%, even after several days. Understanding the factors that limit the rate or extent of hydrolysis is the subject of intense research.[1–3,6,7] Natural cellulose from plants is composed of both crystalline and amorphous regions.[2,8,9] The observed rapid initial rate of digestion was originally thought to be due to hydrolysis of amorphous regions, with the reduced rate that follows resulting from hydrolysis of crystalline material.[1,10–12] However, recent work has shown that the crystallinity index (CrI) does not increase appreciably during enzymatic hydrolysis[13,14] and this hypothesis has been called into question.[1–3] Other contributing factors, such as irreversible nonproductive binding,[15] steric hindrance of bound enzymes at high surface density,[15] and erosion of the surface resulting in loss of productive binding sites,[7,15] have been suggested. In this work we show that, in the presence of agitation, digestion of the material surrounding water-filled nanopores within cellulose fibers occurs rapidly during the initial stage of digestion. This suggests that the initial rapid rate is due, at least in part, to hydrolysis of easily digestable material surrounding the pores. We also show that digestion of the material surrounding the water-filled nanopores does not occur in the absence of agitation, reinforcing the need for well-mixed saccharification reactors operating within a biorefinery.

The structure of cellulose from a variety of sources has been extensively studied in air by small-angle X-ray scattering (SAXS), wide-angle X-ray scattering (WAXS), neutron diffraction, transmission electron microscopy, and scanning probe microscopy.[16–44] Much of this work has involved regenerated or man-made cellulose fibers, whereas the present work focuses on natural crystalline cellulose (Avicel). Natural crystalline cellulose I is composed of elementary fibrils with rectangular

* To whom correspondence should be addressed. E-mail: mskent@sandia.gov.
† Sandia National Laboratories, Albuquerque, NM.
‡ Joint BioEnergy Institute.
§ Sandia National Laboratories, Livermore, CA.
|| Lawrence Berkeley National Laboratory.
⊥ New Mexico State University.
Los Alamos National Laboratories.

10.1021/bm9008952
Published on Web 12/30/2009

cross sections of roughly 25 × 110 Å.[16,34] The structural characteristics of microfibrils formed from elementary fibrils varies with species, but elementary fibrils generally pack into microfibers with diameters ranging up to hundreds of Angstroms.[16,30,34,35,39] The elementary fibrils are composed of crystalline regions separated along the axial direction by amorphous regions.[34,39,42] The long period of the crystalline regions along the fiber axis can range up to several thousand Angstroms.[39] There is also evidence for amorphous regions between microfibrils transverse to the fibril axis.[30]

The distribution of water within cellulose fibers has been studied by solute exclusion,[45] adsorption isotherms,[46] NMR,[47] and small angle neutron scattering (SANS).[48,49] In early work, a solute exclusion technique indicated that pores existed within Solka Floc with an average size less that 4 nm.[45] NMR subsequently confirmed that sorbed water is clustered into pools.[47] The pore size distribution within cotton linter paper was determined using an NMR method based on depression of the freezing point of water within small pores.[47] The results indicated an asymmetric distribution for the pore radius with a maximum in the distribution at 1.4 nm. Additional insight into the structure of the water-filled regions was obtained using NMR spin diffusion methods.[47] Dipolar filter and 2D wide-line separation (WISE) methods suggested that the water pools are surrounded by amorphous cellulose, which in turn is surrounded by crystalline cellulose. The average distance between crystalline domains on opposite sides of a water pool was determined to be 3 nm. Analysis by multilayer fractal BET theory indicated that water sorption significantly alters the local structure of cellulose compared to nitrogen adsorption, and that the distribution of water within the bulk of the material on a nanometer scale can be described by a fractal dimension less than 1.5.[46]

The presence of water-filled pores in paper has also been revealed by SANS measurements.[48,49] The principles of this method are described in the Experimental Section.[50] When deuterated water is used to enhance the scattering contrast with cellulose, the presence of water filled pores results in increased scattered intensity and a roll off of the intensity at high wave vector ($Q = 4\pi \sin\theta/\lambda$, where θ is half the scattering angle and λ is the neutron wavelength). De Spirito et al. showed that these features can be described by a model comprised of small spheres of D_2O in a continuous cellulose matrix.[49] They found that the radius of the water-filled pores ranged from 1.6 to 2.0 nm, increasing with the extent of aging of the paper. These features declined in magnitude when the contrast between water and cellulose was reduced using a mixture of H_2O and D_2O, proving that the features indeed arise from pools of water within the cellulose matrix.

We report the first study of enzymatic hydrolysis of cellulose by SANS. Digestions were performed in a static mode (material settled from aqueous suspensions) and also in flowing aqueous suspensions or dynamic mode. We show that only in the dynamic mode do enzymes digest on a fine scale throughout the microcrystalline cellulose and alter the structure of the water-filled pores.

Experimental Section

Materials. The cellulose substrate in these studies was Avicel FD100 from FMC Biopolymer (Philadelphia, PA) and was used as received. A cellulase enzyme extract from *T. viride* (TV), with an activity of 9 units/mg solid as reported by the manufacturer, and β-glucosidase (β-GC) from almonds, with an activity of 25.7 units/mg solid, were purchased from Sigma-Aldrich (St. Louis, MO). Both TV and β-GC were supplied as dry powders that were subsequently dissolved in buffer. D_2O 99.9% was purchased from Cambridge Isotopes (Andover, MA). The 50 mM sodium acetate buffer was made by dissolving sodium hydroxide (Sigma-Aldrich) in water and adjusting the pH to 5.0 with acetic acid (Sigma-Aldrich).

Table 1. List of the Digestion Conditions[a]

label	wt % FD100	wt % TV	wt % β-GC	T (°C)	mode
S-1	2.0	0.5	0.0	55	static, A
S-2	2.0	0.1	0.0	55	static, A
S-3	2.0	0.1	0.02	55	static, A
S-4	28	0.8	0.0	40	static, B
S-5	27	2.7	0.0	40	static, B
D-1	2.0	0.2	0.0	55	dynamic
D-2	2.0	0.2	0.0	55	dynamic[b]
D-3	2.0	0.2	0.0	55	dynamic[c]
D-4	0.5	0.05	0.02	40	dynamic

[a] The static digestions were performed at the wt % FD100 given above, but the SANS measurements were performed at the settled concentration which was much higher. [b] FD100 circulated at 55 °C for 12 h prior to start of study. [c] FD100 processed with a high shear mixer and fractionated prior to start of study.

Methods. *Background Information for Neutron Scattering.* In this method, a collimated neutron beam is delivered to the sample. The diameter of the neutron beam incident on the sample ranges from 8 to 12 mm, and sample thickness is typically 1−2 mm. A two-dimensional, position sensitive detector detects the scattered neutrons. For an isotropic, two-dimensional scattering pattern, radial averaging is performed and the data is reduced to a one-dimensional form, which is subsequently put on an absolute scale using either a standard sample or a direct measurement of the absolute beam intensity. The reduced data are reported as the differential cross section per unit solid angle per unit volume, $d\Sigma(Q)/d\Omega = I(Q)$ (cm^{-1}) as a function of the scattering vector, Q (defined above). Here we also normalize the SANS data to solute volume fraction, Φ, for direct comparison of different samples. The shape of the scattering curve gives information on the structure, $\rho(r)$, of the sample. $\rho(r)$ is the position-dependent scattering length density (SLD) in the sample, which is defined as the sum of scattering lengths, b, for all atoms in an arbitrary volume, V, at r, divided by the volume. For particles suspended in a medium, the scattered intensity can be factored into a term due to the size, shape, and internal structure of the particles (namely, the form factor $P(Q)$), a term due to the interaction among the particles (namely, the structure factor $S(Q)$), and a term due to the contrast, $\Delta\rho$, between the particles and the medium (for example, a solvent). The contrast arises from the differences in the SLD at different r. These considerations give for a collection of interacting spherical particles

$$\frac{d\Sigma(Q)}{d\Omega} = N_p \Delta\rho^2 V_p^2 P(Q) S(Q) \quad (1)$$

where N_p is the number density of the particles in a medium and V_p is the volume of one particle. The Q domain measured in a SANS experiment is typically from 0.001 to 0.5 $Å^{-1}$, which determines the length scale ($\sim 1/Q$) of the detectable amorphous structural features to be roughly 10−1000 Å. For crystalline structure, the length scale in the Bragg relation is given as $2\pi/Q$. The ultrasmall-angle neutron scattering (USANS) measurement extends the Q domain to about 2×10^{-5} $Å^{-1}$, corresponding to length scales of order 5 μm. Structural features less than 10 Å cannot be reliably obtained due to the interference of the incoherent background produced mostly from protons in the sample.

Next we describe the protocols used for the SANS studies of digestion in static and dynamic modes.

Digestion Procedures. The conditions for all digestions are listed in Table 1.

Static Digestion: Method A. Eppendorf tubes (50 mL) containing identical suspensions of Avicel FD100 and cellulase enzymes in buffer were placed in a water bath at 55 °C. Cellulose and enzyme concentrations are given in Table 1. No agitation was used so the FD100

settled to the bottom of the tubes. Individual tubes were removed after various periods of time and placed in a refrigerator (5 °C), quenching the hydrolysis. After the end of the digestion period, all the refrigerated samples were centrifuged and the supernatant of each tube was removed for analysis of reducing sugar content. The pellets were then resuspended in D_2O buffer and centrifuged again. The process of resuspension and centrifugation was repeated five times to ensure nearly complete exchange of D_2O buffer for H_2O buffer. A sample of as-received FD100 was also suspended in D_2O buffer.

The SANS sample cells were loaded with the cellulose suspensions in D_2O buffer and the solids allowed to settle. After settling, the supernatant was removed and additional suspension was added. This process was repeated until the scattering cell was filled with a sufficiently high solids content, typically ~10−20 wt % cellulose, such that negligible further settling occurred. SANS data for a cell containing pure D_2O buffer was collected and subtracted as background from the data for the samples containing cellulose in proportion to the buffer volume fraction.

SANS and USANS measurements for static digestions were performed at the National Institutes of Standards and Technology Center for Neutron Research (NG7 SANS and BT5 beamlines) and at Los Alamos National Laboratory (Low-Q Diffractometer, LQD). Measurements on NG7 and BT5 were performed using standard 1 or 2 mm path length stainless steel cells with quartz windows. On NG7, scattering data were obtained at three detector distances to achieve a range of Q from 0.003 to 0.6 $Å^{-1}$. Measurements on LQD were performed using quartz cuvettes of 1 and 2 mm path length. LQD operates in the time-of-flight mode, and scattering data were obtained for a fixed sample to detector distance over a wavelength range from 2 to 15 Å. The data from NG7 were placed on an absolute scale, $d\Sigma(Q)/d\Omega$ (cm^{-1}), by measuring the absolute intensity of the incident beam. The data from LQD were placed on an absolute scale by reference to the scattering from a standard sample.

Following the SANS measurements, the concentration of solids in each scattering cell was determined by removing the material from the cells, recording the weight, drying the material in a vacuum oven at 70 °C, and then recording the dried weight.

Static Digestion: Method B. FD100 Avicel was mixed with buffer at ~28 wt % along with cellulase enzymes, yielding a paste-like consistency. The mixture was stirred briefly and then immediately injected into a scattering cell. Measurements were initiated within 10−20 min of mixing, and scans were repeated until no further changes were detected. Data for a cell containing pure D_2O buffer was collected and subtracted as background from the data for the samples containing cellulose in proportion to the buffer volume fraction.

Dynamic Digestions. SANS measurements for dynamic digestions were performed at the High Flux Isotope Reactor at Oak Ridge National Laboratory (Bio-SANS) and at National Institutes of Standards and Technology (NG7). The cellulose dispersion in buffer was continuously circulated at a flow rate of 20 mL/min through a 1 mm path length sample cell (Hellma 170-000-120 or Hellma 137-1-40) during SANS measurements using a peristaltic pump and Teflon tubing (1/16 in ID). The circulation system also included a 5 mL vial to serve as a reservoir. The vial contained a magnetic stirring bar and was heated to the desired temperature with a water bath. The stirring rate was in all cases set close to the maximum rate that allowed for stable stirring. The actual rates varied as different stirring plates were used at different locations but were in the range 600−800 rpm. A metal block holding the Hellma cell was also heated to the desired temperature. Negligible settling was observed over the duration of the measurements. Initially the circulation system was charged with a 2 wt % dispersion of FD100 in buffer. After scans were completed at three sample-to-detector distances (0.3, 6, and 14.5 m for Bio-SANS; 1.0, 4.5, and 13 m for NG7), cellulase enzymes were added (Table 1) and scans were repeated at regular intervals at 0.3 and 6 m (Bio-SANS) or 1.0 and 4.5 m (NG7). The duration of the in situ digestion measurements ranged from 8 to 20 h. Final scans were then performed at all three sample-to-detector distances. Scans for a cell containing pure D_2O buffer were also collected and subtracted as background from the data for the samples containing cellulose. The data from HFIR were placed on an absolute scale by reference to the scattering from a standard sample.

Assays of Sugar Yields. Samples were removed from static and dynamic digestions at various times, centrifuged, and the supernatant was retained for analysis of reducing sugars. Yields of reducing sugars released upon digestion were determined using the colorimetric assay of Nelson−Somogyi.[51] Glucose concentrations were measured using an Agilent 1200 HPLC (Santa Clara, U.S.A.) equipped with a Varian 380LC Evaporative Light Scattering Detector (Varian Inc., Palo Alto, CA). Separation was achieved using a Carbomix Pb-NP Column carbohydrate analytical column (300 × 7.7 mm, 5 μm, 8% cross-linking) with a guard column (50 × 7.7 mm) at 85 °C (Sepax Technologies Inc., Delaware, U.S.A.) with a mobile phase of deionized water flowing at 0.5 mL/min. External monosaccharide standards, ranging between 1 and 20 mM, were used to determine concentrations.

Measurement of the Amount of Protein Adsorbed. In selected assays the amount of protein adsorbed was determined by measuring the concentration of protein in the supernatant by absorbance at 280 nm. Cellulose solutions were centrifuged (3000 rpm, 5 min) and the supernatants were removed and analyzed using a JASCO J-815 spectrometer. Absolute concentrations were determined by reference to a standard measurement of a known concentration of the enzyme extract prepared from the dry powder.

X-ray Diffraction. In selected cases, static and dynamic digestions were halted at various times and the residual solids were isolated by centrifugation. The samples were scanned on a Siemens D500 $\theta-\theta$ diffractometer equipped with a sealed tube Cu Kα source, diffracted-beam graphite monochromator, and scintillation detector. Scans were collected from $2\theta = 4-60°$ with a step size of 0.05 degrees at 4 s per step. The crystallinity index was determined as $[I\,(22.5°) - I\,(18°)]/I\,(22.5°) \times 100$.[52]

Fluorescence Microscopy. Fluorescence images of cellulose particles with adsorbed enzymes were obtained using an Olympus IX71 spinning disk confocal fluorescence microscope. TV enzymes were labeled using the amine reactive dye Alexa-488 tetrafluorophenylester (Invitrogen). Labeled enzymes were mixed at 5% with unlabeled enzymes. Samples were removed from static and dynamic digestions after 10 min and 1 h. The samples were centrifuged (12000 rpm for 5 min) and washed with buffer three times to remove unbound enzymes. The particles were then dispersed in buffer, deposited onto a glass slide, and imaged at 1 μM resolution in depth and 1.2 μM resolution in-plane at an exposure of 300 ms.

SEM Micrographs. SEM images were obtained for selected samples from static and dynamic digestions. The analyses of samples from the static and dynamic digestions occurred roughly a year apart, and different microscopes were used in the two cases. For analysis of the samples from the static digestion, samples were prepared by drop casting 10 μL of sample onto a silicon chip and drying under nitrogen at ambient temperature. The samples were subsequently coated with approximately 180 Å of Au/Pd using a Desk II sputtering system. The micrographs were taken with a JEOL JSM-6400FV scanning microscope using an acceleration voltage of 2 kV. For analysis of the samples from the static digestion, the samples recovered from the digestion were centrifuged to recover the residual solids which were then washed with phosphate buffer, dehydrated with ethanol (5 steps), critical point dried (Tousimis Critical Point Drier), and then mounted onto brass sample stubs with carbon tape and sputter coated with Au/Pd. The micrographs were taken at 2 kV on a Hitachi S-5000 microscope.

Results

SANS Measurements. *As-Received Cellulose.* Scattering data for as-received FD100 in weak contrast (30% D_2O buffer, 70% H_2O buffer) and strong contrast conditions (100% D_2O buffer) are shown in Figure 1. The samples were prepared by settling as described in the Methods. This resulted in a settled cellulose

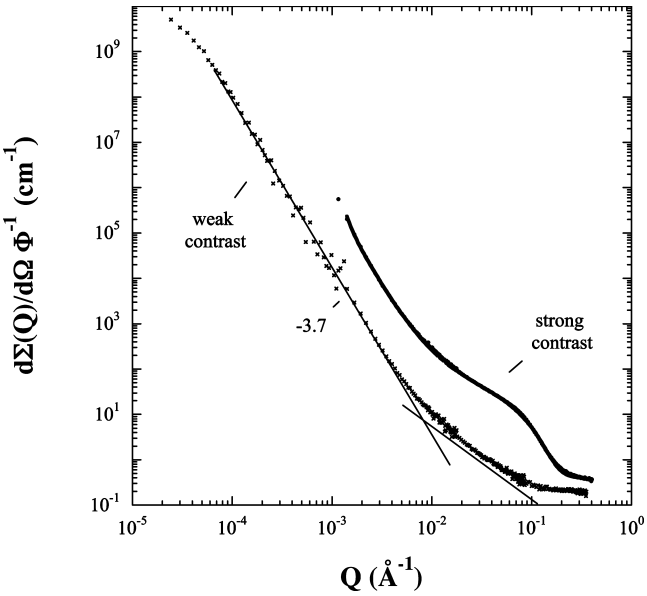

Figure 1. Scattering data for ~20 wt % FD100 in weak contrast conditions (30% D_2O buffer, 70% H_2O buffer, ×) and strong contrast conditions (100% D_2O buffer, ●), along with the best fit of eq 3 in the latter case. SANS and USANS data are combined for the weak contrast condition.

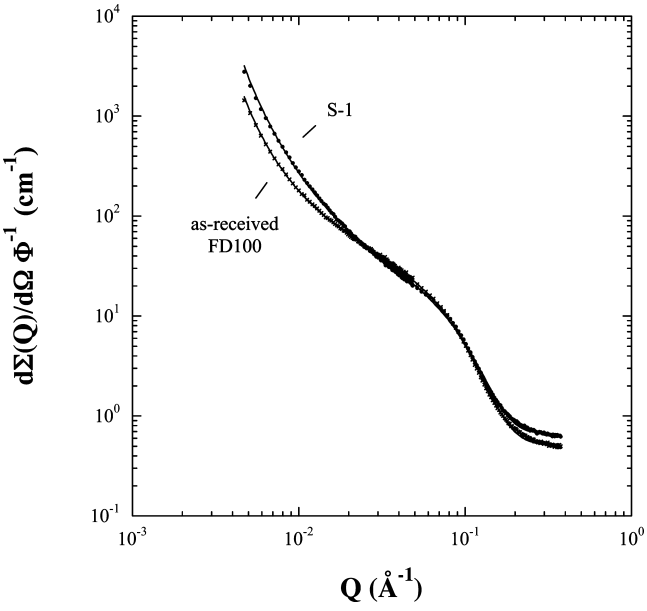

Figure 2. SANS data for digestion S-1 for as-received FD100 (×) and after 60 h of digestion along with best fits of eq 3 (●).

volume fraction of ~20%. For weak contrast conditions, both SANS and USANS data were obtained at this concentration. For strong contrast conditions, USANS data were not useable at this high concentration due to intense multiple scattering. In weak contrast conditions, the scattering curve in Figure 2 is comprised of a region where the intensity decreases monotonically as a power law of $Q^{-3.7}$ for $Q = 10^{-4}$ Å^{-1} to $Q = 10^{-2}$ Å^{-1} and a regime with a much weaker decay from $Q = 10^{-2}$ Å^{-1} to $Q = 10^{-1}$ Å^{-1}. For strong contrast conditions, the data follow a decay for $Q < 4 \times 10^{-3}$ Å^{-1} comparable to that obtained in weak contrast conditions over the same Q range. However, for $Q > 4 \times 10^{-3}$ Å^{-1} excess intensity is present and a distinct knee or roll off in intensity occurs at $\sim Q = 0.08$ Å^{-1} that is not observed at weak contrast. As mentioned earlier, the excess scattering and roll off have previously been identified as due to water-filled pores within the cellulose fibers.[47–49] The fact that the increased intensity and roll-off disappear in weak contrast (30% D_2O, 70% H_2O), where the SLD is close to that of cellulose, demonstrates that water penetrates into the pores throughout the entire sample.

Our analysis follows closely that outlined previously by De Spirito et al.[49] They proposed that neutron scattering data from hydrated cellulose fibers can be described by the sum of contributions from the network of crystalline cellulose microfibrils and from water pools trapped within the amorphous regions, along with an incoherent term (B_{inc}):[49]

$$d\sum(Q)/d\Omega = A_1 S(Q)_1 P(Q)_1 + A_2 S(Q)_2 P(Q)_2 + B_{inc} \quad (2)$$

where $S(Q)_i$ and $P(Q)_i$ are the structure factor and form factors for the cellulose fibrils ($i = 1$) and the water pools ($i = 2$). The prefactors A_1 and A_2 are proportional to the square of the difference in SLD between water and cellulose and the concentrations of fibers and water pools, respectively. Because the diameter of the cellulose fibers (d) is large in relation to $1/Q$, $S_1(Q) \approx 1$ and the only contribution observable in the SANS data from $P_1(Q)$ will be from the fiber surface structure. These are the same approximations used by De Spirito et al. Therefore, we interpret the low-Q power law as reflecting the scattering for fractal-like surfaces $P(Q)$ α Q^{D_1}, where D_1 is related to the surface "fractal" dimension D_s by $D_1 = D_s - 6$. Moreover, from the same assumption the prefactor A_1 will be proportional to the total exposed surface area of the fibers. Modeling the water pools as spheres of radius R with a log-normal distribution of radii, $f(R)$, and distributed with a mass fractal dimension D_2 up to a cutoff dimension, ξ, gives the scattering as[49]

$$d\sum(Q)/d\Omega = A_1 Q^{D_1} + A_2 P(Q)\{1 + \beta[S(Q) - 1]\} + B_{inc} \quad (3)$$

$$S(Q) = 1 + \frac{1}{(QR)^{D2}} \frac{D_2\Gamma(D_2 - 1)}{[1 + 1/Q^2\xi^2]^{(D_2-1)/2}} \times \sin[(D_2 - 1)a\tan(Q\xi)]$$

$$P^*(Q) = V^2 P(Q) = \langle |F(Q)|^2 \rangle,\ \beta = |\langle F(Q) \rangle|^2 / \langle |F(Q)|^2 \rangle$$

$$\langle |F(Q)|^2 \rangle \int_0^\infty |F(Q)|^2 f(R) dR,\ |\langle F(Q) \rangle|^2 = |\int_0^\infty F(Q) f(R) dR|^2$$

$$f(R) = \frac{1}{\sigma R\sqrt{2\pi}} \exp\left[-\frac{1}{2\sigma^2}(\ln(R) - \mu)^2\right]$$

$$F(Q) = \left[\frac{3[\sin(QR) - QR\cos(QR)]}{(QR)^3}\right]$$

where $F(Q)$ is the form factor for a sphere, $\mu = \ln(R_{med})$, where R_{med} is the median radius, and σ is the standard deviation of the variable's (R) natural logarithm.[53] The averaged spherical form factor results in the knee-like feature. In eq 3 the rather simple form for the influence of interparticle interactions on the scattering introduced in eq 1 for a distribution of interacting spheres is replaced by a decoupling approximation that allows for polydispersity in R.

The assumption of a spherical shape for the water pores is an important simplification leading to the simple analytical expression in eq 3. This is almost certain to be only a crude approximation, yet despite that fact, eq 3 adequately describes our results for as-received Avicel FD100, as shown by the quality of the fit to the data for strong contrast conditions in Figure 1. Of primary importance is that there is substantial

Table 2. Parameters from Fits with Eq 3

	wt % FD100	mode	R_{avg} (nm)	σ	A_1 (cm^{-1})	D_1	D_2
Figure *1*	20	static, A	1.7	0.32	1.0e−5	3.5	1.4
Figure *2* (no TV)	30	static, A	1.6	0.37	5.4e−6	3.5	1.3
Figure *2* (60 h)	30	static, A	1.7	0.31	1.2e−5	3.5	1.4
Figure *3* (no TV)	30	static, B	1.7	0.30	5.4e−6	3.5	1.3
Figure *3* (60 h)	30	static, B	1.7	0.30	2.8e−5	3.3	1.7
Figure *4* (no TV)	2	dynamic	1.7	0.37	2.9e−5	3.5	1.9
Figure *4* (45 min)			0.6	0.62	2.9e−5	3.5	2.1
Figure *5* (no TV)	2	dynamic	1.5	0.41	2.2e−5	3.6	2.0
Figure *5* (1 h 20 m)			0.5	0.70	2.2e−5	3.6	2.1
Figure S1 (no TV)	2	dynamic	1.8	0.37	3.4e−5	3.6	2.1
Figure S2a (no TV)	2	static, A	1.7	0.32	1.0e−5	3.5	1.4
Figure S2a (20 h)	2	static, A	1.9	0.22	2.5e−5	3.4	1.7
Figure S5 (no TV)	2	dynamic	2.3	0.24	3.1e−5	3.4	2.0

correlation in the shape and size of the pores. The data are not sensitive to the precise geometrical shape due to many factors that smear out the effects of higher resolution features in the data. The fitted parameters are $R_{avg} = 1.7$ nm, $D_1 = 3.5$, and $D_2 = 1.4$, which are comparable to the values reported previously in a SANS study of newly fabricated paper ($R_{avg} =$ 2.0 nm, $D_1 = 3.7$, and $D_2 = 1.6-1.7$).[49] The value of D_2 obtained here is also in good agreement with the previously reported value obtained from multilayer BET analysis of water adsorption isotherms of Avicel.[46]

As discussed below, over later stages of dynamic digestion, the signal characteristic of the pores disappeared and was replaced by a simple power law; thus, eq 3 was only used to fit data for the as-received fibers, static digestion, and the earliest stages of dynamic digestion.

SANS data were also obtained from an FD100 sample after processing with a high shear mixer and subsequent fractionation to recover the low molecular weight fraction. The average particle size of that sample was ~40 times smaller than that of as-received FD100. The shape of the scattering curve (Supporting Information, Figure S1) was similar to that of the as-received material. This shows that, on the length scale probed by SANS (10−1000 Å), the structure was largely unaffected by processing with the high shear mixer.

In another experiment, SANS data were obtained for FD100 at 2 wt % in D_2O buffer as-received and after circulating in the flow system for 12 h at 55 °C in the absence of enzymes. There was no detectable change in shape of the scattering curve following this treatment.

Static Digestions. SANS data for static digestion S-1 after 60 h (Method A) are shown in Figure 2 along with data for as-received FD100. The best-fits using eq 3 are also shown. Scattering curves for 2, 20, and 40 h of digestion (not shown) were nearly identical to the curve for 60 h. In static Method A, unbound enzymes were removed during the exchange of H_2O buffer for D_2O buffer. Data for static digestions S-2 and S-3 are shown in Figure S2 (Supporting Information). The trends in the scattering are qualitatively similar for the three series despite the fact that the extent of digestion varied considerably. The extent of digestion after 24 h was greater for S-1 (~30 mM reducing sugar released) than for S-2 (~20 mM reducing sugar released) due to higher enzyme loading. For comparison, complete conversion of 2 wt % cellulose to glucose would yield a concentration of 123 mM. Digestions S2 and S3 differ only in the concentration of β-GC. At high concentrations, the hydrolysis product cellobiose inhibits the activity of cellulase enzymes.[1,54] The presence of β-GC decreases the extent of this inhibition by hydrolyzing cellobiose to glucose. Whereas the addition of β-GC at 0.02 wt % (S-3) increased the yield of reducing sugars at 24 h by 5 mM, it had no effect on the form of the scattering data.

Two changes were observed in the SANS data for the partially digested samples relative to that for as-received FD100. The main effect was an increase in scattering for 0.003 Å^{-1} < Q < 0.03 Å^{-1}. This effect did not increase monotonically with digestion time, but rather was present in the measurement of the sample removed 2 h after enzyme addition and was nearly the same for samples removed after that. The parameters from the best-fit of eq 3 to the data in Figure 2 and Figure S2a are given in Table 2. The results indicate that the increase in scattering for 0.003 Å^{-1} < Q < 0.03 Å^{-1} is due mainly to an increase in A_1. The increased scattering most likely reflects an increase in surface area as large particles are broken down into many smaller fragments. Optical micrographs indicate a substantial decrease in average particle size for the 2 h sample relative to the as-received material with little change after that. The SANS data and optical micrographs thus indicate that most of the small particle generation occurred within the first 2 h for the static digestions. This simply reflects that fact that most of the digestion occurred during the first few hours, after which the rate of digestion leveled off.

The second change observed for the partially digested samples is that the level of incoherent scattering obtained from the plateau at the highest Q values is increased. This incoherent

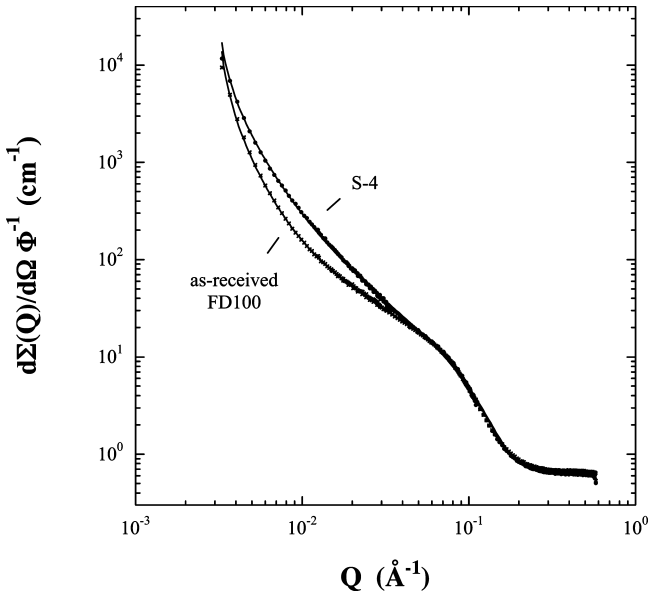

Figure 3. SANS data for digestion S-4 for as-received FD100 (×) and after 8 h of digestion along with best-fits of eq 3 (●).

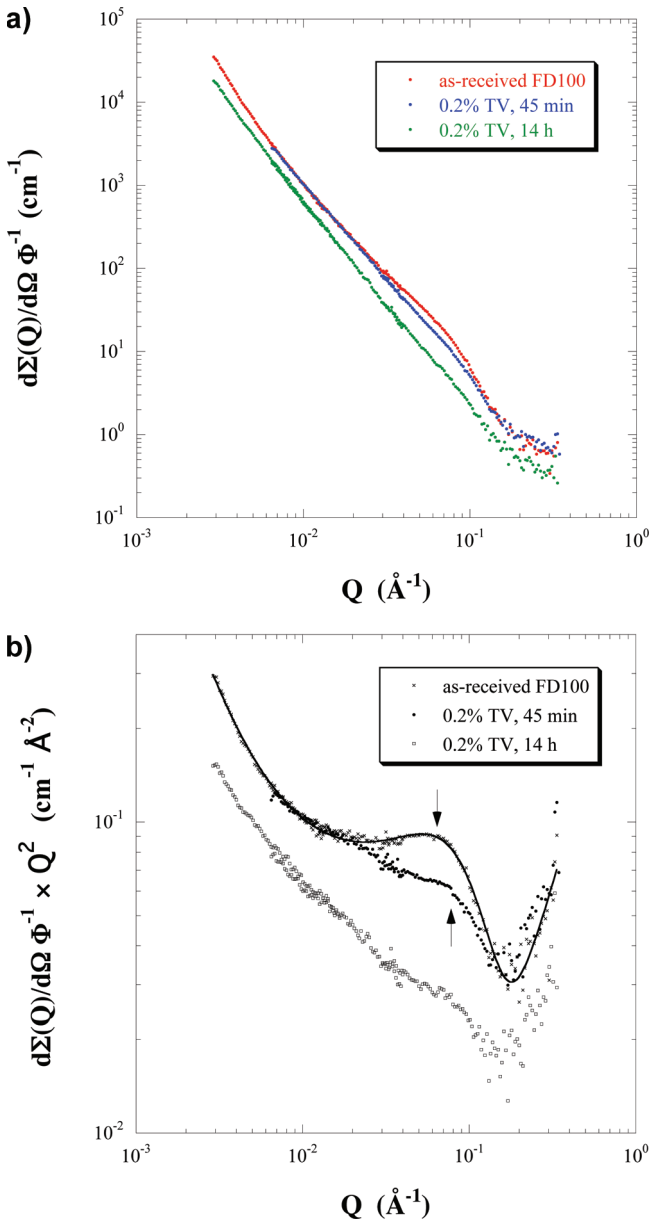

Figure 4. SANS data for digestion D-1 along with the best-fit of eq 3 to the data for as-received Avicel.

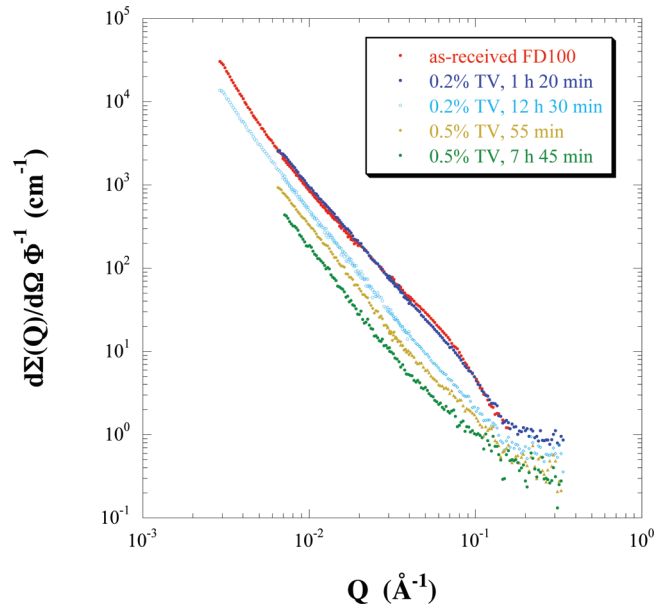

Figure 5. SANS data for digestion D-2.

scattering comes mainly from hydrogen atoms in the sample and likely results from incomplete exchange of H_2O buffer for D_2O buffer.

SANS results for static digestion S-4 at 40 °C performed by static method B at 28 wt % FD100 and 0.8% TV are shown in Figure 3 along with best-fits to eq 3. In this case, free enzymes were present during the measurement, but independent measurement of the enzymes in D_2O buffer alone indicated that their contribution was negligible (Supporting Information, Figure S3). Once again, after addition of enzymes an increase in scattering was observed for 0.003 Å^{-1} < Q < 0.03 Å^{-1}. The extent of digestion was much lower for S-4 compared with S-1 (<1% based on theoretical glucose compared with 27%), presumably due to the much higher concentration of cellobiose in S-4. Despite the very low extent of digestion, the increase in scattering for 0.003 Å^{-1} < Q < 0.03 Å^{-1} after addition of enzymes is greater in Figure 3 than in Figure 2. This can be explained by the fact that in digestion S-1 some very fine particles of cellulose may have been lost from the sample during the centrifugation and supernatant recovery process, whereas all particles were retained in the in situ digestion S-4. The parameters from the best-fit of eq 2 to the data again indicate that the increase in scattering for 0.003 Å^{-1} < Q < 0.03 Å^{-1} is due to an increase in A_1. R_{avg} of the water-filled pores remained at 17 Å with polydispersity of 0.3.

To summarize the results for static digestions, an increase in coherent scattered intensity was observed in the lower Q region of the measured range that is attributed to an increase in total surface area resulting from the generation of small particles. Significantly, the SANS data indicate that enzyme activity does not occur within or around the water-filled pores, despite an appreciable overall enzyme activity of ~20−30%. The lack of change in intensity at higher Q values also suggests that enzymes do not penetrate into the water-filled pores. At higher Q values the scattered intensity reflects the structure of water-filled pores inside the microfibers and is proportional to the contrast between the two. Penetration of enzymes into the pores would have displaced D_2O. Displacement of D_2O by protonated enzymes would have caused a reduction in contrast between the pores and the microfibers and decreased intensity. Figure 1 demonstrates the limiting case in which no contrast exists between the pores and the surrounding microfibril matrix.

Dynamic Digestions. SANS data for dynamic digestion D-1 with 2 wt % FD100 and 0.2 wt % TV at 55 °C are shown in Figure 4a. For a relatively narrow pore size distribution, scattering from the correlated water pools leads to a peak in the intensity when plotted as $d\Sigma(Q)/d\Omega \times Q^2$ versus Q,[49] amplifying the changes observed in this feature with digestion (Figure 4b). Data are shown for scans taken prior to injecting enzymes and at 45 min and 14 h after injecting TV. The parameters from the best-fit of eq 3 to the data prior to injecting enzymes and 45 min after injecting enzymes are given in Table 2. Prior to injecting enzymes, the average pore radius and polydispersity are consistent with the measurements made in the static mode. However, in contrast to the data for the static digestions, the high Q roll off decreased substantially within 45 min of injecting enzymes. Furthermore, the scattered intensity over lower Q values dropped substantially over the course of digestion, in contrast to the results for the static digestions where only increased intensity was observed. The decrease in scattered intensity at low Q indicates a decrease of scattering mass and

hence surface area as digestion proceeds. In the data collected 45 min after injecting enzymes, the intensity in the region of the high Q roll off is weaker and has shifted slightly to higher Q relative to the curve for as-received FD100. This is shown more clearly in Figure 4b. For the best fit with eq 3, the average pore radius has decreased to 0.6 nm. As mentioned earlier, eq 3 was not used to fit data after substantial periods of digestion, but rather the data were analyzed in terms of power laws. After 14 h of digestion, the scattering follows a power law decay with exponent -2.48 ± 0.01 over most of the Q range.

Figure 5 shows SANS data for enzymatic digestion D-2 with 2 wt % FD100 and 0.2 wt % TV at 55 °C. In this case, the mixing and circulation system was charged with FD100 and circulated for 12 h at 55 °C prior to the SANS study. The purpose of this was to determine if stirring and circulation at 55 °C in absence of enzymes affects the structure or digestibility of the cellulose fibers. In Figure 5, SANS data are shown for scans taken prior to injecting enzymes and also at 1 h 20 min and 12 h 30 min after injecting TV at 0.2 wt %. After injecting enzymes, qualitatively similar changes in the data are observed as for the data for D-1 in Figure 4. Parameters resulting from fits of the data before injecting enzymes and 1 h 20 min after injecting enzymes are given in Table 2. Again, early in the digestion process a decrease is observed in the average radius of the water-filled pores. After 20 h of digestion, the scattering follows a power law decay with exponent -2.50 ± 0.01 over most of the Q range. After 20 h, a second addition of TV enzymes was made that increased the total concentration to 0.5 wt %. Scans were then repeated for an additional 5 h.

At higher Q values, the changes in the scattering patterns with digestion in Figures 4 and 5 reflect changes in the distribution of water internal to the fibers. This follows from the data in Figure 1. The lower intensity and shift to higher Q of the high Q roll off and its disappearance as digestion proceeds in Figures 4 and 5 indicate substantial changes occur in the structure of the water-filled pores. In both digestion series, the roll-off shifted to higher Q early in the digestion process, and fitting with eq 3 results in an average pore radius that is smaller than that for the as-received material (see Table 2). This can be explained by rapid enzymatic digestion in or around the larger pores but lack of digestion around the smaller pores. In that case, digestion around the larger pores would decrease their contribution to the scattering, while scattering from the smaller pores would remain. Lack of digestion around the smaller pores is to be expected if access to the smaller pores is limited by the size of the enzymes. Our measurements indicate average pore diameters ranging from 3.2−3.6 nm. Other measurements indicate an asymmetric pore size distribution skewed to larger pores.[47] From this, only a fraction of the pores should be accessible to cellulase enzymes (estimated size ~ 5 nm).[55]

Another important observation is that, following the loss of scattering from the pores (hump in Figure 4b), the intensity versus Q follows a power law over much of the Q range with an exponent that increases in absolute magnitude as digestion proceeds (Figure 6). The power law exponents reflect the changing spatial distribution of water inside the fibers. However, interpretation of power law exponents in terms of structure is complicated by the fact that different structures can give the same power law exponent. Nevertheless, often useful qualitative trends and comparisons can still be made.

Fractals are a class of objects that result in a power law dependence of the scattered intensity on Q, $I \sim Q^{D}$.[56] Mass "fractal" dimensions and surface "fractal" dimensions can be distinguished based on the exponent value, with values of $D =$ −3 to −4 corresponding to surface dimensions (−4 corresponding to smooth, −3 corresponding to rough) and absolute values less than 3 corresponding to mass "fractal" dimensons. For mass fractals, the absolute value of the exponent decreases as the mass distribution becomes less compact. Some nonfractal mass distributions can also result in power law scattering. For example, mass distributed in a random walk as for polymer chains in a theta solvent corresponds to an exponent of −2. An exponent of −2 also results for large thin sheet-like objects. Polydisperse systems and asymmetric particles can in some instances also exhibit power law scattering.

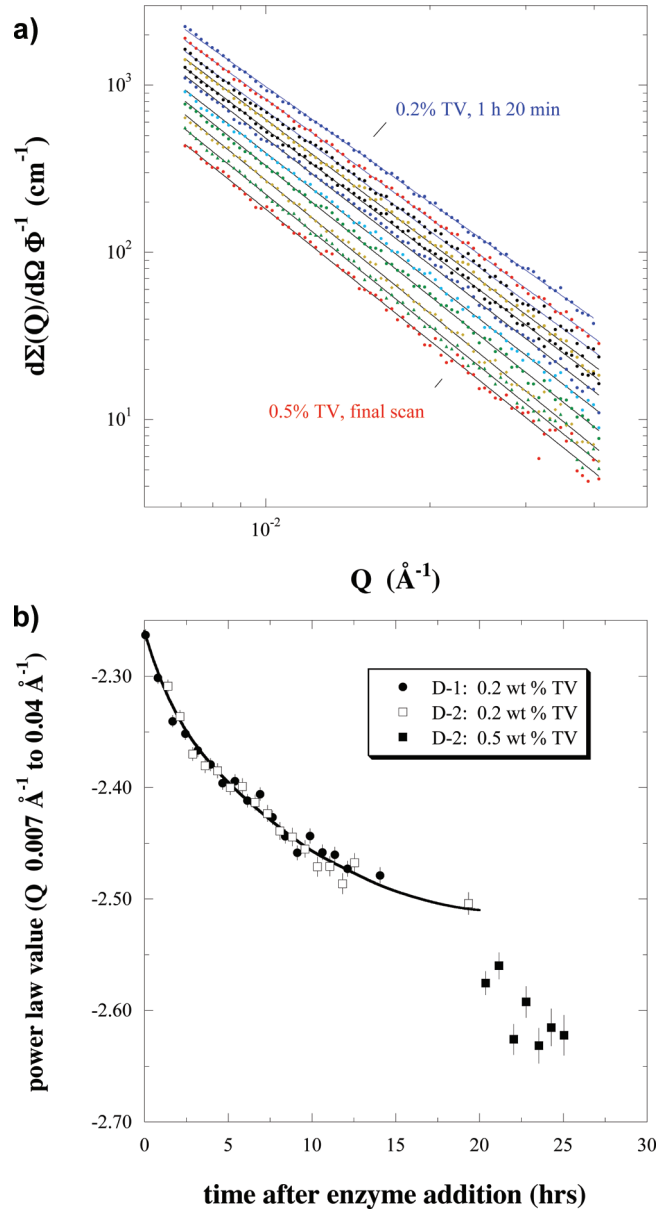

Figure 6. (a) Expanded view of successive SANS scans for 0.007 Å^{-1} < Q < 0.04 Å^{-1} for D-2 along with best-fits to a power law decay. (b) Values of apparent power law exponents as a function of time after enzyme addition for D-1 and D-2.

Power law exponents for digestions D-1 and D-2 over the Q range 0.007 Å^{-1} < Q < 0.04 Å^{-1} are given in Figure 6b. The increase in absolute magnitude of the power law exponents corresponds to a more compact or dense distribution of water inside the fibers as digestion proceeds. This is expected as the pores grow in size and coalesce to form larger pools. Quantitative comparison of such data for different enzyme systems or

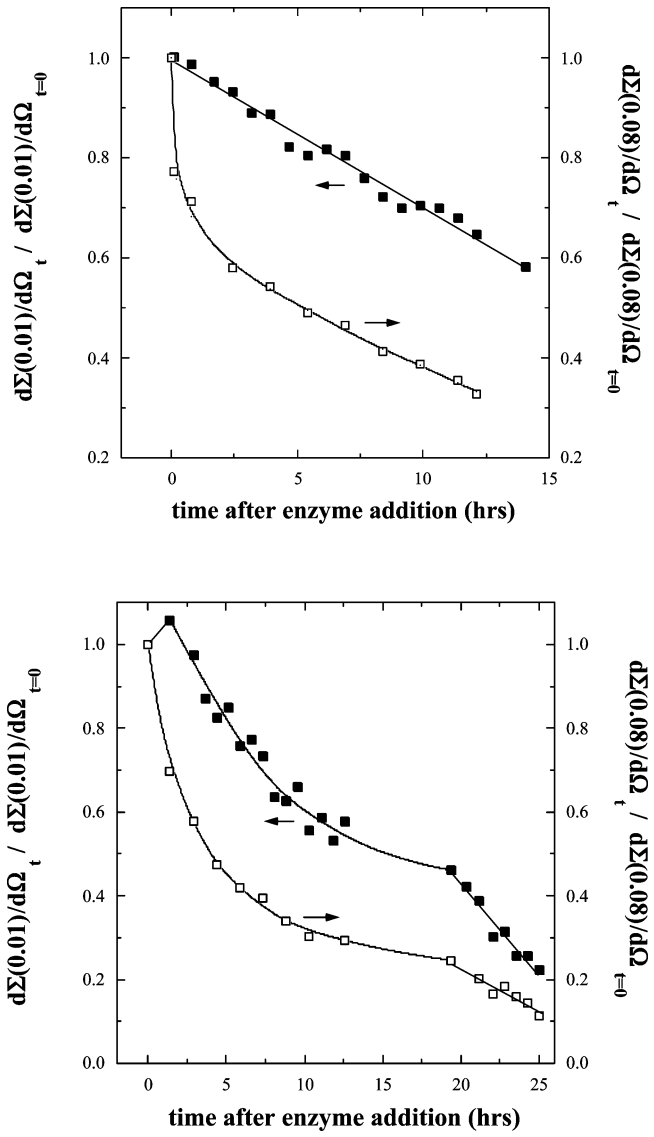

Figure 7. Scattered intensity at $Q = 0.01$ Å^{-1} (■) and $Q = 0.08$ Å^{-1} (□) as a function of time after addition of enzymes for (a) D-1 and (b) D-2. The more rapid decay at $Q = 0.08$ Å^{-1} indicates a much faster time scale for loss of scattering from the form factor of the water-filled pores.

conditions should reveal the relative activity of enzymes internal to the fibers.

Additional information is provided by comparing the time dependence of the intensity at specific Q values. Figure 7 displays the absolute intensity at $Q = 0.01$ Å^{-1} and at $Q = 0.08$ Å^{-1} as a function of digestion time for D-1 and D-2. The intensity at $Q = 0.08$ Å^{-1} reflects the scattering from the form factor of the water-filled pores. The more rapid decrease in the scattered intensity at $Q = 0.08$ Å^{-1} is a result of enzyme digestion around the pores. The trend in the intensity at $Q = 0.01$ Å^{-1} for D-2 is different than that for D-1, indicating that the 12 period of circulation at 55 °C prior to addition of enzymes had a small effect on the interaction of enzymes with the substrate, despite the fact that no structural change was detected in the SANS data prior to enzyme addition. For D-2, the intensity at $Q = 0.01$ Å^{-1} initially increased upon enzyme addition (see also Figure 5) followed by a more rapid decrease in intensity with time than in D-1. Earlier we argued that the increase in intensity for 0.003 Å^{-1} < Q < 0.03 Å^{-1} in the static digestions is most likely due to increased surface area that results from the breakup of large particles. The initial increase in intensity at $Q = 0.01$ Å^{-1} for D-2 then suggests that in the initial stages of digestion the generation of small particles occurs more rapidly than digestion of the same, such that total surface area increases. Following the initial increase, the more rapid decrease in intensity at $Q = 0.01$ Å^{-1} compared with the data for D-1 suggests that the prior period of circulation made the material more amenable to digestion. Finally, upon addition of further enzymes after 20 h in D-2, a marked change in slope occurred indicating that addition of fresh enzyme immediately increased the rate of digestion.

In addition to the two dynamic digestions discussed above, two additional dynamic digestions were performed. In one case (D-3), FD100 was processed with a high shear mixer and fractionated prior to digestion. The sample was loaded into a flow cell system at 2 wt % and digested for 8 h with 0.2 wt % TV at 55 °C. The SANS data, shown in Figure S1 (Supporting Information), also show loss of the high Q roll off as for the data in Figures 4 and 5. Dynamic digestion D-4 was performed at lower loadings of FD100 and enzymes (0.5 wt % FD100, 0.05 wt % TV, and 0.02 wt % b-GC) for 8 h at 40 °C. The data, shown in Figure S4 (Supporting Information), once again show loss of the high Q roll off upon digestion. The data also show an increase in intensity for Q < 0.03 Å^{-1} after addition of enzymes, as was observed for D-2. This indicates that small particle generation and digestion around the pores occurred simultaneously. For D-4, the digestion did not proceed to as great an extent as for D-1 or D-2 due to the lower temperature and lower enzyme loading.

Electron Micrographs. SEM images have been reported previously for Avicel.[46] SEM micrographs of FD100 as a function of digestion time are shown in Figure S5 (Supporting Information) for static digestion S-2 and in Figure S6 (Supporting Information) for dynamic digestion D-1. No changes on a fine scale are evident upon digestion for either digestion mode in these micrographs. This is not unexpected as the length scale of the water-filled pores is much smaller than can be detected by SEM.

Extent of Digestion. The amount of FD100 recovered as a solid by centrifugation after 24 h of digestion of 2 wt % FD100 with 0.5 wt % TV was 8 ± 5% for dynamic digestions and 78 ± 7% for static digestions (averages of 3 runs). This shows that for a given time period digestion proceeds to a far greater extent in the dynamic mode compared with the static mode. This was confirmed in the quantity of sugars released. The static digestions under these conditions yielded 19 mM glucose (HPLC) after 24 h, whereas the dynamic digestions released 84 mM glucose in the same time period. The corresponding values of reducing sugars from the Nelson−Somogyi assay were 44 and 114 mM, respectively. Complete conversion to glucose corresponds to 123 mM. A representative plot of reducing sugar concentration (Nelson−Somogyi assay) over time for static and dynamic digestions at 0.2 wt % TV is given in Figure S7 (Supporting Information).

Enzyme Adsorption. In selected cases, the amount of enzyme adsorbed as a function of digestion time was determined for both static and dynamic digestions by measuring the concentration of enzyme in the supernatant. Comparison at 2 wt % FD100 and 0.5 wt % TV, shown in Figure 8, shows that in both static and dynamic digestions enzyme adsorption occurs very rapidly and reaches a comparable maximal adsorbed amount (minimum concentration remaining in the supernatant) shortly after introducing the enzymes. Fluorescence microscopy images of cellulose particles removed from static and dynamic

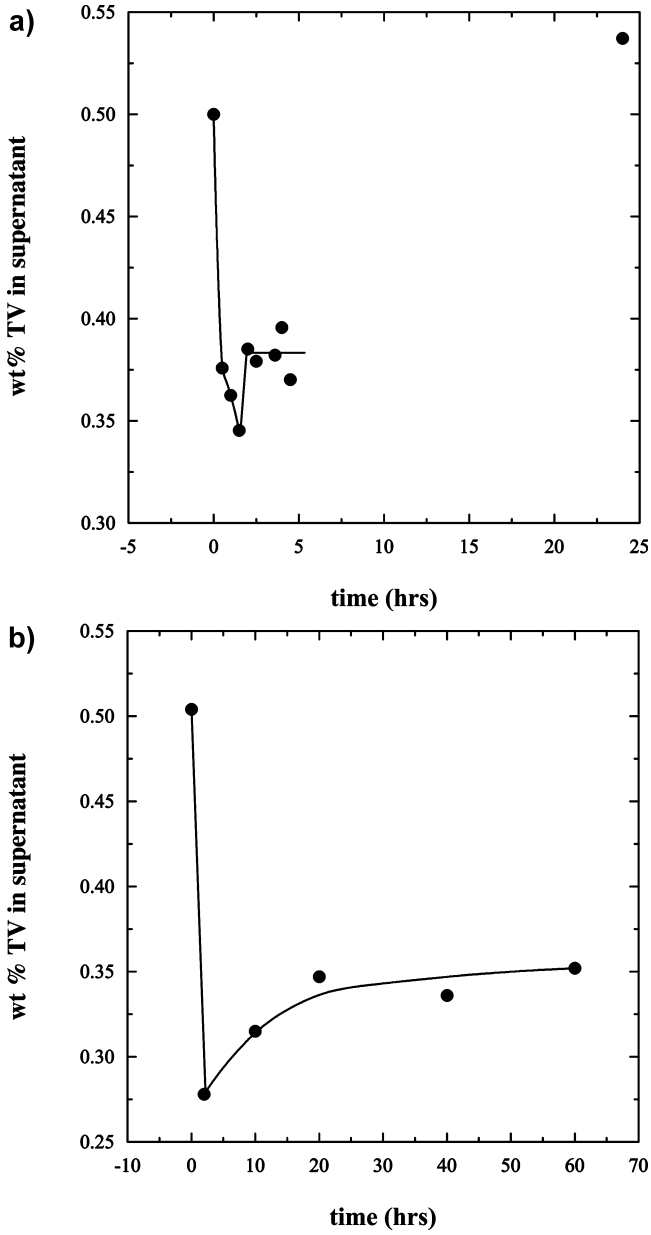

Figure 8. Concentration of enzyme in the supernatant as a function of digestion time for (a) static digestion and (b) dynamic digestion. The initial amounts of FD100 and TV were 2 and 0.5 wt %, respectively.

digestions shown in Figure S8 (Supporting Information) also show that the overall level of enzyme adsorption is comparable. In addition, the images at ~1 μm resolution show no difference in enzyme distribution within the particles.

X-ray Diffraction. The CrI of FD100 was measured by XRD for samples as-received, after 24 h static digestion at 0.5 wt % TV, and after 6 and 24 h dynamic digestion at 0.5 wt % TV. The values were 89, 89, 88, and 90%, respectively, with an uncertainty of ±3% in each case. Thus, no change in the crystalline fraction upon digestion was detected for either mode.

Discussion

Upon addition of enzymes, the SANS data for the dynamic digestions show rapid loss of the roll off at $Q = 0.08$ Å^{-1} and decreased intensity over the entire Q range, effects that are absent for the static digestions even after 60 h. These findings

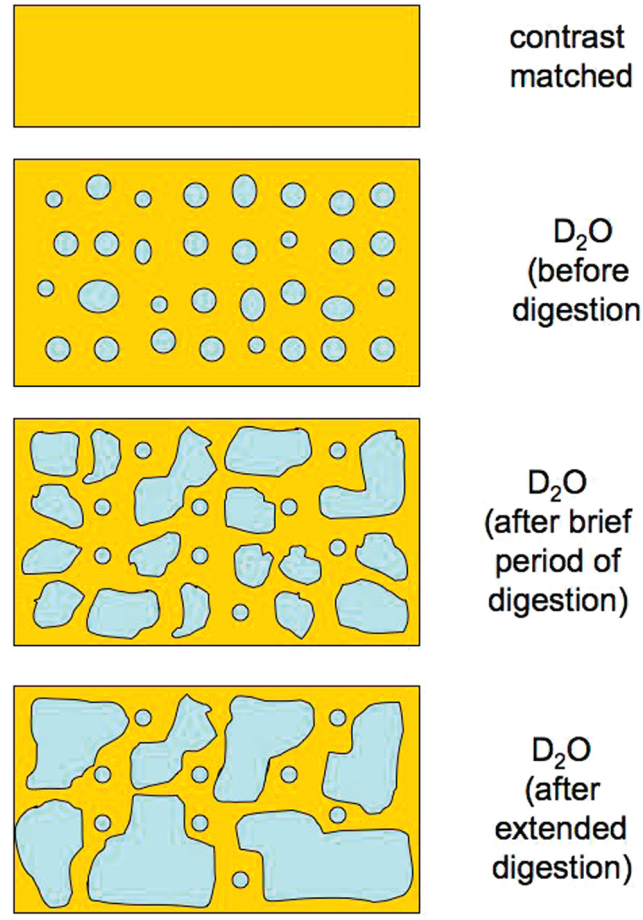

Figure 9. Illustration of structural interpretation of the SANS data for the dynamic digestions.

indicate that the structure of the water-filled pores is altered in the dynamic digestions but not in the static digestions. The fact that the loss of the scattering contribution from the water-filled pores occurs early in the digestion suggests that this reflects the cause of enhanced digestion rather than being simply a consequence of enhanced digestion. It is important to note that the decreased scattering from the pores is a synergistic effect due to the presence of enzymes combined with agitation. No change in the fine structure occurred after 12 h in the dynamic system in the absence of enzymes or upon processing with a high shear mixer, and likewise, no effect was detectable when enzymes were present in absence of mixing and flow (static digestion, Figure 2).

Our interpretation of the high Q scattering data is illustrated in Figure 9. Hydrated, as-received FD100 contains water-filled pores with a fairly narrow size distribution as observed previously in paper.[47] In the dynamic case, enzymes are able to digest the regions surrounding the larger water pools. This in turn leads to broadening of the pore size distribution and probably also a loss of regularity in the shape of the pools. Either effect would lead to a loss of the scattering contribution from the pores. However, we postulate that enzymes are unable to penetrate the smallest pores and these remain unaffected for much of the digestion process. This explains the shift in the hump to higher Q values in Figure 4b and the corresponding decrease in average pore size obtained from the fits.

The scattering data at high Q thus indicate that in the presence of agitation, enzyme activity occurs on a different structural level, at the level of nanopores, than occurs in the absence of agitation. Moreover, the very rapid disappearance of the

contribution to the scattering from the form factor of the water-filled voids in the dynamic case indicates that at the earliest stages digestion occurs around the pores throughout the bulk of the sample. One possible explanation for the difference in behavior is that only in the presence of agitation do the enzymes penetrate the fibers to a fine level and access the water-filled nanopores. However, the data for enzyme depletion in the supernatant and the fluorescence microscopy images do not support this interpretation in that the amount and initial rate of adsorption were comparable for static and dynamic digestions. If enzymes had penetrated the fibers to a fine level only in the dynamic digestions then the initial adsorbed amount would have been much greater in that case. Alternatively, enzymes may access the pores to the same extent in both static and dynamic modes but become rapidly inhibited by cellobiose in the static case due to limited mass transport of the small molecule product away from the surface.

We note that, due to settling, the local concentration of cellulose fibers in the static digestions was much higher than in the dynamic digestions. The higher local concentration of cellulose fibers would also serve to increase cellobiose concentration and inhibit enzyme activity. We were unable to reach concentrations above 5% in the circulating system due to increased viscosity and partial gelation and so we cannot determine the extent to which digestion would occur around the pores in that case.

In a prior study, Lee and Fan considered the presence of nanopores of diameter <40 Å in developing a kinetic model for enzymatic hydrolysis of cellulose (Solka Floc).[54,57] They observed that enzymes adsorbed very rapidly to the surface of cellulose and that the amount of adsorbed enzyme within the first 15 min was identical for stirring rates of 0 and 250 rpm. From the rapid rate of adsorption and the lack of dependence of the adsorbed amount on stirring rate, they concluded that enzymes do not penetrate into the nanopores. They argued that the average size of cellulase enzymes would not permit their diffusion into the nanopores and, thus, that digestion does not occur within the nanopores. Although our data for enzyme depletion in the supernatant also show rapid adsorption and lack of a strong dependence of the adsorbed amount on stirring rate, the scattering data clearly show that the enzymes alter the structure of the larger pores in the dynamic case. We note that the present results do not directly indicate the level of enzyme penetration, but show only that the larger water-filled pores are altered by digestion in the presence of agitation. The enzymes may act from outside the pores or at the edges rather than from inside the pores. While penetration of enzymes into the D_2O-filled pores would lower the SLD and therefore could in principle be observed directly, this cannot be resolved in the present data for the dynamic digestions because of rapid digestion of the material surrounding the pores. This could be resolved in the future through the use of inactivated enzymes or binding modules that lack a catalytic domain.

Following the loss of scattering from the pores, the time dependence of the power law exponents reveals the changing spatial distribution of water internal to the fibers, showing an increasingly dense and compact distribution as digestion proceeds. The decrease in intensity at low Q in the dynamic digestions indicates a decrease in total surface area and possibly also increased roughness of fiber surfaces. The loss of mass is a consequence of an extended period of active digestion. We note that the decrease in intensity at low Q in the dynamic digestions occurs on a much longer time scale than the loss in the contribution from the pore form factor.

The increased rate of digestion upon addition of fresh enzyme after 20 h in the case of D-2 suggests that the enzymes are not irreversibly bound. The increased rate would appear to be due to the fresh enzymes replacing nonproductive original enzymes. This question is the focus of ongoing work.

While subjecting the cellulose to a 12 h period of circulation and mixing at 55 °C prior to addition of enzymes had little or no affect on the structure of the water-filled pores, it did slightly enhance the digestability of the material. It is possible that this treatment affected the structure on a larger length scale than probed by SANS; for example, it may have partially degraded the surface layer of the cellulose fibers.

Finally, the present results may bear upon a discussion in the literature regarding changes in reactivity of Avicel with digestion. Two groups have attempted to determine the relative reactivity of Avicel with respect to cellulase enzymes at different stages of digestion by stopping the digestion, removing bound enzyme, and then measuring the initial activity after addition of fresh enzymes.[58,59] This determines the substrate reactivity at a given extent of conversion, which is an intrinsic property of the substrate determined by structural characteristics such as area accessible to cellulase, surface roughness, number of free ends, degree of polymerization, and so on. One group concluded that the substrate reactivity was approximately constant with conversion whereas a second group reported a sharp drop in substrate reactivity with conversion. We note that enzyme loading and stirring rate varied significantly between the two studies. SANS is one of very few techniques that can provide structural details of the cellulose fibers during the digestion process. Our data for the agitated system shows that enzymes access the regions in or around the nanopores from the start, and digest those regions very rapidly. This correlates well with the rapid decline in substrate reactivity reported by one group.[59] Together, these findings suggest that the material surrounding the pores is more easily digestable than the remaining material, resulting in a decrease in substrate reactivity as digestion proceeds. However, because no change in CrI was detected throughout the digestion, the more easily digestable material surrounding the pores must include both amorphous and crystalline regions.

Conclusions

We report the first neutron scattering study of enzymatic digestion of cellulose fibers. In the absence of enzymes, at low Q ($Q < 0.004$ Å^{-1}), the particles scatter as dense solids with rough surfaces, and the Q dependence of the scattering reflects the surface "fractal" dimensional characteristics of the fibers. The observed power law exponent of -3.7 corresponds to a surface fractal dimension of 2.3. At higher Q, the scattering data is sensitive to the internal structure of the fibers. In particular, in strong contrast conditions, the higher Q scattering data reflects the distribution of water inside the particles. For the as-received fibers, excess scattering and a roll off in intensity result from water-filled pores of relatively narrow size distribution as reported previously.[47−49]

For digestions performed in the absence of stirring or flow (static digestions), the extent of digestion was limited to roughly 30% in 24 h for the conditions of this study. The excess intensity and high Q roll off remained unaffected by digestion. An increased intensity was observed at lower Q that is likely due to increased surface area resulting from breakup of the large agglomerates or surface erosion. The lack of change in the high

Q roll off suggests that the enzymes act on regions between or at the surface of the fibers but that the enzymes do not digest the regions surrounding the pores.

In digestions that included agitation in the form of rigorous stirring and flow (dynamic), digestion proceeded to a much greater extent. The scattering attributed to distinct water-filled pores was rapidly lost, indicating digestion around the larger nanopores throughout the volume of the fibers. The intensity at low *Q* decreased as digestion proceeded, indicating the loss of scattering mass.

We suggest that in the static case the enzymes become rapidly inhibited by cellobiose due to limited mass transport of the small molecule product, leading to limited digestion. This could be especially pronounced in the confined environment of the nanopores. The higher local concentration of cellulose in the static samples could also contribute to increased product inhibition. In the future, insight into the distribution of enzymes throughout the material could be provided by SANS through the use of deuterium enriched enzymes.

Prior studies have shown that stirring enhances digestion, but the present SANS study has revealed that only in the presence of agitation do enzymes digest on a fine scale and alter the structure of the water-filled pores.

Acknowledgment. This work was part of the DOE Joint BioEnergy Institute (http://www.jbei.org) supported by the U.S. Department of Energy, Office of Science, Office of Biological and Environmental Research, through Contract DE-AC02-05CH11231 between Lawrence Berkeley National Laboratory and the U.S. Department of Energy. Sandia is a multiprogram laboratory operated by Sandia Corporation, a Lockheed Martin Company, for the United States Department of Energy under Contract DE-AC04-94AL85000. We acknowledge the support of the National Instititute of Standards and Technology, U.S. Department of Commerce, the High Flux Isotope Reactor (HFIR) at the Oak Ridge National Laboratory, and the Los Alamos Neutron Science Center (LANSCE) at the Los Alamos National Laboratory in providing neutron research facilities used in this work. HFIR and LANSCE are sponsored by the Scientific User Facilities Division, Office of Basic Energy Sciences, U.S. Dept. of Energy.

Supporting Information Available. SANS data for digestions D-3, D-4, S2, S3, and S5. Scanning electron micrographs of material from static digestion S-1 and dynamic digestion D-1. Plot of reducing sugar concentration versus time for static and dynamic digestions at 2 wt % FD100, 0.2 wt % TV, 55 °C. Confocal fluorescence microscopy images of cellulose particles removed from static and dynamic digestions at 2 wt % FD100, 0.1 wt % TV, 55 °C. This material is available free of charge via the Internet at http://pubs.acs.org.

References and Notes

(1) Mansfield, S. D.; Mooney, C.; Saddler, J. N. *Biotechnol. Prog.* **1999**, *15*, 804–816.
(2) Zhang, Y. H. P.; Lynd, L. R. *Biotechnol. Bioeng.* **2004**, *88*, 797–824.
(3) Zhang, Y. H. P.; Himmel, M. E.; Mielenz, J. R. *Biotechnol. Adv.* **2006**, *24*, 452–481.
(4) Lynd, L. R.; Laser, M. S.; Bransby, D.; Dale, B. E.; Davison, B.; Hamilton, R.; Himmel, M.; Keller, M.; McMillan, J. D.; Sheehan, J.; Wyman, C. E. *Nat. Biotechnol.* **2008**, *26*, 169–172.
(5) Grabber, J. H.; Ralph, J.; Lapierre, C.; Barriere, Y. C. R. *Biologies* **2004**, *327*, 455–465.
(6) Jeoh, T.; Wilson, D. B.; Walker, L. P. *Biotechnol. Prog.* **2006**, *2006*, 270–277.
(7) Eriksson, T.; Karlsson, J.; Tjerneld, F. *Appl. Biochem. Biotechnol.* **2002**, *101* (1), 41–60.
(8) O'Sullivan, A. C. *Cellulose* **1997**, *4*, 173–207.
(9) Muller, M.; Czihak, C.; Schober, H.; Nishiyama, Y.; Vogl, G. *Macromolecules* **2000**, *33*, 1834–1840.
(10) Fan, L. T.; Lee, Y. H. *Biotechnol. Bioeng.* **1981**, *23*, 419–424.
(11) Fan, L. T.; Lee, Y. H.; Beardmore, D. H. *Biotechnol. Bioeng.* **1980**, *22*, 177–199.
(12) Lee, S. B.; Kim, I. H.; Ryu, S. S. Y.; Taguchi, H. *Biotechnol. Bioeng.* **1983**, *25*, 33–51.
(13) Lenze, J.; Esterbauer, H.; Sattler, W.; Schurz, J.; Wrentschur, E. *J. Appl. Polym. Sci.* **1990**, *41*, 1315–1326.
(14) Sinitsyn, A. P.; Gusakov, A. V.; Vlasenko, E. Y. *Carbohydr. Polym.* **1991**, *10*, 1–14.
(15) Valjamae, P.; Sild, V.; Pettersson, G.; Johansson, G. *Eur. J. Biochem.* **1998**, *253* (2), 469–75.
(16) Frey-Wyssling, A. *Science* **1954**, *119*, 80–82.
(17) Heyn, A. N. *J. Appl. Phys.* **1955**, *5*, 1113–1120.
(18) Kratky, O.; Miholic, G. *J. Polym. Sci., Part C* **1963**, *2*, 449–476.
(19) Heyn, A. N. *J. Ultrastruct. Res.* **1969**, *26*, 52–68.
(20) Scallan, A. M. *Text. Res.* **1971**, *41*, 647–653.
(21) Hindeleh, A. M.; Johnson, D. J. *Polymer* **1972**, *13*, 423–430.
(22) Nomura, T.; Yamada, T. *Wood Res.* **1972**, *52*, 1–12.
(23) Haase, J.; Hosemann, R.; Renwanz, B. *Kolloid. Z. Z. Polym.* **1973**, *251*, 871–875.
(24) Haase, J.; Hosemann, R.; Renwanz, B. *Colloid Polym. Sci.* **1974**, *252*, 712–717.
(25) Blackwell, J.; Kolpak, F. J. *Macromolecules* **1975**, *8*, 322–326.
(26) Fengel, D. *Holzforschung* **1978**, *32*, 37–44.
(27) Boylston, E. K.; Hebert, J. J. *J. Appl. Polym. Sci.* **1980**, *25*, 2105–2107.
(28) Nishimura, H.; Okano, T.; Asano, I. *Mokuzai Gakkaishi* **1982**, *28*, 659–668.
(29) Fink, H.-P.; Fanter, D.; Phillip, B. *Acta Polym.* **1985**, *36*, 1–8.
(30) Misra, T.; Bisoyi, D. K.; Patel, T.; Patra, K. C.; Patel, A. *Polym. J.* **1988**, *20*, 739–749.
(31) Lenz, J.; Schurz, J.; Wrentschur, E. *J. Appl. Polym. Sci.* **1988**, *35*, 1987–2000.
(32) Fink, H.-P.; Hofmann, D.; Purz, H. J. *Acta Polym.* **1990**, *41*, 131–137.
(33) Jakob, H. F.; Fratzl, P.; Tschegg, S. E. *J. Struct. Biol.* **1994**, *113*, 13–22.
(34) Jakob, H. F.; Fengel, D.; Tschegg, S. E.; Fratzl, P. *Macromolecules* **1995**, *28*, 8782–8787.
(35) Zhang, Y. Z.; Chen, X. L.; Liu, J.; Gao, P. J.; Shi, D. X.; Pang, S. J. *J. Vac. Sci. Technol., B* **1997**, *15*, 1502–1505.
(36) Crawshaw, J.; Cameron, R. E. *Polymer* **2000**, *41*, 4691–4698.
(37) Entwistle, K. M.; Navaranjan, N. *J. Mater. Res.* **2002**, *37*, 539–545.
(38) Sjiligoj Smole, M.; Persin, Z.; Kreze, T.; Stana Kleinschek, K.; Ribitsch, V.; Neumayer, S. *Mater. Res. Innovations* **2003**, *7*, 275–282.
(39) Yu, H.; Liu, R.; Shen, D.; Wu, Z.; Huang, Y. *Carbohydr. Polym.* **2008**, *72*, 122–127.
(40) Nishiyama, Y.; Langan, P.; Chanzy, H. *J. Am. Chem. Soc.* **2002**, *124*, 9074–9082.
(41) Lai-Kee-Him, J.; Chanzy, H.; Muller, M.; Putaux, J. L.; Imai, T.; Bulone, V. *J. Biol. Chem.* **2002**, *277*, 36931–36939.
(42) Bhattacharya, D.; Germinario, L. T.; Winter, W. T. *Carbohydr. Polym.* **2008**, *73*, 371–377.
(43) Sugiyama, M.; Hara, K.; Hiramatsu, N.; Iijima, H. *Jpn. J. Appl. Phys.* **1998**, *37*, L404–L405.
(44) Fischer, E. W.; Herchenroder, P.; Manley, R. S. J.; Stamm, M. *Macromolecules* **1978**, *11*, 213–217.
(45) Van Dyke, B. H. *Enzymatic hydrolysis of cellulose—A kinetic study*; Massachusetts Institute of Technology, Cambridge, MA, 1972.
(46) Stromme, M.; Mihranyan, A.; Ek, R.; Niklasson, G. *J. Phys. Chem. B* **2003**, *107*, 14378–14382.
(47) Capitani, D.; Proietti, N.; Ziarelli, F.; Segre, A. L. *Macromolecules* **2002**, *35*, 5536–5543.
(48) Missori, M.; Mondelli, C.; De Spirito, M.; Castellano, C.; Bicchieri, M.; Schweins, R.; Arcovito, G.; Papi, M.; Castellano, C. *Phys. Rev. Lett.* **2006**, *97*, 238001−1–238001−4.
(49) De Spirito, M.; Missori, M.; Papi, M.; Maulucci, G.; Teixeira, J.; Castellano, C.; Arcovito, G. *Phys. Rev. E* **2008**, *77*, 041801−1–041801−9.
(50) Higgins, J. S.; Benoit, H. C. *Polymers and Neutron Scattering*; Oxford University Press: Oxford, 1996; Vol *8*.
(51) Green, F.; Clausen, C. A.; Highley, T. L. *Anal. Biochem.* **1989**, *182*, 197–199.

(52) Segal, L.; Creely, J. J.; Martin, A. E., Jr.; Conrad, I. C. M. *Text. Res. J.* **1959**, *29*, 786–794.
(53) Kotlarchyk, M.; Chen, S.-H. *J. Chem. Phys.* **1983**, *79*, 2461–2469.
(54) Fan, L. T.; Lee, Y. H. *Biotechnol. Bioeng.* **1983**, *25*, 2707–2733.
(55) Ishizawa, C. I.; Davis, M. F.; Schell, D. F.; Johnson, D. K. *J. Agric. Food Chem.* **2007**, *55*, 2575–2581.
(56) Raper, J. A.; Amal, R. *Part. Part. Syst. Charact.* **1993**, *10*, 239–245.
(57) Lee, Y. H.; Fan, L. T. *Biotechnol. Bioeng.* **1982**, *24*, 2383–2406.
(58) Yang, B.; Willies, D. M.; Wyman, C. E. *Biotechnol. Bioeng.* **2006**, *94*, 1122–1128.
(59) Hong, J.; Ye, X.; Zhang, Y. H. P. *Langmuir* **2007**, *23*, 12535–12540.

BM9008952